J|A|C|S
ARTICLES
Published on Web 03/26/2004

Carbon Nanotube Synthesis in Supercritical Toluene

Doh C. Lee, Frederic V. Mikulec, and Brian A. Korgel*

Contribution from the Department of Chemical Engineering, Texas Materials Institute, Center for Nano- and Molecular Science and Technology, The University of Texas at Austin, Austin, Texas 78712-1062

Received December 4, 2003; E-mail: korgel@mail.che.utexas.edu

Abstract: Multiwall carbon nanotubes (MWNTs) were synthesized in supercritical toluene at 600 °C and ~12.4 MPa using ferrocene, Fe, or FePt nanocrystals as growth catalysts. Toluene serves as both the carbon source for nanotube formation and the solvent. In contrast to vapor-phase synthetic routes, the supercritical solvent provides high precursor concentration and a homogeneous reaction environment with dispersed growth catalyst particles. Both carbon filaments and MWNTs are produced by this approach, and a growth mechanism is proposed to explain the factors that determine the nanotube versus filament morphology. The plasmon energies of the π and $\pi + \sigma$ valence electrons were measured using electron energy-loss spectroscopy (EELS) of individual carbon fibers and MWNTs as a characterization tool to complement the imaging data obtained from electron microscopy.

Introduction

Carbon nanotubes exhibit a variety of unique properties, which make them suitable for many potential uses, including structural, electronic, and optical applications.[1] The commercial use of carbon nanotubes in real-world applications requires a cost-effective method to fabricate large amounts of nanotubes with the desired material properties. With only a couple of exceptions,[2−4] carbon nanotube formation has been explored exclusively in the gas phase using synthetic methods such as arc-discharge,[5] laser vaporization,[6] and chemical vapor deposition (CVD),[7] because they provide access to the high synthetic temperatures required for nanotube formation. Under the extremely high temperature conditions of arc-discharge and laser vaporization (2000−4000 °C), carbon atoms can be vaporized from a solid carbon target and condensed into high-quality single-wall nanotubes. The relatively low yield, high operational costs, and low throughput of these methods, however, limit their potential use as a manufacturing approach for large-scale nanotube production.

Metal catalysts have enabled high-quality carbon nanotube synthesis at much lower temperatures (500−1200 °C) using hydrocarbon species as reactants in conventional CVD reactors.[8−10] Metal-catalyzed decomposition of CO to carbon nanotubes had been observed as early as 1955;[11] however, not until recently have researchers embarked on a concerted effort to produce high-quality nanotubes by metal-catalyzed CVD.[12,13] Andrews et al.,[14] for example, have produced high-quality MWNTs by CVD at 625−775 °C and atmospheric pressure using ferrocene to catalyze the decomposition of aromatic compounds to nanotubes. In comparison to vapor-phase synthetic methods, supercritical fluid-phase approaches have the potential for much higher throughput due to orders-of-magnitude higher precursor concentration and catalyst particle dispersibility, which would enable a continuous homogeneous synthetic process. Since carbon nanotube synthesis requires high temperatures (>600 °C), the solvents must be pressurized to achieve this temperature range. Solvents at high pressures and temperatures—above their critical points—have been used to synthesize a variety of materials[15−17] and more recently have played an important role in the synthesis of a variety of nanostructures.[18−24]

(1) Dresselhaus, M. S., Dresselhaus, G., Avouris, P., Eds. *Carbon Nanotubes: Synthesis, Structure, Properties, and Applications*; Springer: New York, 2002.
(2) Gogotsi, Y.; Libera, J. A.; Yoshimura, M. *J. Mater. Res.* **2000**, *15*, 2591−2594.
(3) Libera, J.; Gogotsi, Y. *Carbon* **2001**, *39*, 1307−1318.
(4) Shao, M.; Li, Q.; Wu, J.; Xie, B.; Zhang, S.; Qian, Y. *Carbon* **2000**, *40*, 2961−2973.
(5) Ebbesen, T. W.; Ajayan, P. M. *Nature* **1992**, *358*, 220−222.
(6) Thess, A.; Lee, R.; Nikolaev, P.; Dai, H.; Petit, P.; Robert, J.; Xu, C. H.; Lee, Y. H.; Kim, S. G.; Rinzler, A. G.; Colbert, D. T.; Scuseria, G. E.; Tomanek, D.; Fischer, J. E.; Smalley, R. E. *Science* **1996**, *273*, 483−487.
(7) Ren, Z. F.; Huang, Z. P.; Xu, J. W.; Wang, J. H.; Bush, P.; Siegal, M. P.; Provencio, P. N. *Science* **1998**, *282*, 1105−1107.
(8) Dai, H.; Kong, J.; Zhou, C.; Franklin, N.; Tombler, T.; Cassell, A.; Fan, S.; Chapline, M. *J. Phys. Chem. B* **1999**, *103*, 11246−11255.
(9) Delzeit, L.; Nguyen, C. V.; Chen, B.; Stevens, R.; Cassell, A.; Han, J.; Meyyappan, M. *J. Phys. Chem. B* **2002**, *106*, 5629−5635.
(10) Hofmann, S.; Ducati, C.; Robertson, J.; Kleinsorge, B. *Appl. Phys. Lett.* **2003**, *83*, 135−137.
(11) Hofer, L. J. E.; Sterling, E.; McCarthy, J. T. *J. Phys. Chem.* **1955**, *59*, 1153−1155.
(12) Nikolaev, P.; Bronikowski, M. J.; Bradley, R. K.; Rohmund, F.; Colbert, D. T.; Smith, K. A.; Smalley, R. E. *Chem. Phys. Lett.* **1999**, *313*, 91−97.
(13) Bronikowski, M. J.; Willis, P. A.; Colbert, D. T.; Smith, K. A.; Smalley, R. E. *J. Vac. Sci. Technol., A* **2001**, *19*, 1800−1805.
(14) Andrews, R.; Jacques, D.; Qian, D. L.; Rantell, T. *Acc. Chem. Res.* **2002**, *35*, 1008−1017.
(15) Gogotsi, Y. G.; Yoshimura, M. *Nature* **1994**, *367*, 628−630.
(16) Hubert, H.; Garvie, L. A. J.; Devouard, B.; Buseck, P. R.; Petuskey, W. T.; McMillan, P. F. *Chem. Mater.* **1998**, *10*, 1530−1537.
(17) Barns, R. L.; Freeland, P. E.; Kolb, E. D.; Laudise, R. A.; Patel, J. R. *J. Cryst. Growth* **1978**, *43*, 676−686.
(18) Watkins, J. J.; Blackburn, J. M.; McCarthy, T. J. *Chem. Mater.* **1999**, *11*, 213−215.
(19) Ziegler, K. J.; Doty, R. C.; Johnston, K. P.; Korgel, B. A. *J. Am. Chem. Soc.* **2001**, *123*, 7797−7803.

We have recently developed a supercritical fluid−liquid−solid (SFLS) approach to synthesize various semiconductor nanowires, including Si,[20,24] Ge,[22,23] and GaAs.[25] Sterically stabilized metal nanocrystals are input as seed particles that direct wire growth at temperatures that exceed the metal/semiconductor eutectic temperature, which is approximately 360 °C for Au:Ge and Au:Si. The temperature must be sufficiently high to degrade the molecular precursor and to induce nanowire formation. In this paper, we present the synthesis of multiwall carbon nanotubes in supercritical toluene, catalyzed by ferrocene, or nanocrystals of Fe or FePt. In this process, toluene serves as both the carbon source for nanotube growth and the reaction solvent. Under the synthetic conditions producing the highest quality nanotubes, toluene degrades catalytically at the metal particle surfaces, with only minimum homogeneous toluene degradation. MWNTs ranging from 10 to 50 nm in outer diameter with wall thicknesses ranging from 5 to 40 nm were produced along with carbon nanofilaments. High-resolution transmission electron microscopy (HRTEM) reveals that although the MWNT growth mechanism exhibits similarities to SFLS growth, the processes are distinct: the morphology of the nanotubes appears to depend on the growth catalyst, with larger particles producing solid nanofilaments and smaller particles yielding MWNTs. Furthermore, nanotube growth appears to occur on the catalyst particle surface. The nanotubes were characterized by HRTEM, HRSEM, and electron energy loss spectroscopy (EELS). EELS of individual MWNTs and filaments provided a particularly powerful tool for distinguishing MWNTs from carbon nanofilaments.

Experimental Section

Synthesis. Anhydrous toluene, ferrocene, and hexane were purchased from Aldrich Chemical Co. (Milwakee, MI), stored under nitrogen, and used as received. Fe nanocrystals were synthesized by thermal decomposition of iron pentacarbonyl ($Fe(CO)_5$) (Aldrich) in octyl ether (Fluka) in the presence of oleic acid (Fluka) as a cappling ligand at 100 °C, following published procedures.[26] FePt nanocrystals were prepared by thermal decomposition of platinum acetylacetonate ($Pt(CH_3COCCHCH_3)_2$) (Aldrich) and iron pentacarbonyl ($Fe(CO)_5$) in the presence of oleic acid and oleylamine (Aldrich).[27]

Carbon nanotubes were synthesized in a high-pressure 10 mL stainless steel reactor. Solutions of toluene and catalyst were loaded into the reactor in a nitrogen-filled glovebox. In the case of ferrocene, 0.1, 2.5, and 5 mM toluene solutions were prepared and tested, and the nanocrystal concentration was set to 2.5 mM. The volume of the solutions was adjusted so that the pressure determined from the toluene phase diagram[28] should be ∼12.4 MPa. Note that extreme care must be taken not to exceed the pressure rating on the reactor, as the pressure−density isotherm rises sharply just above the critical point and small deviations in volume can lead to large increases in pressure. For example, for a reaction carried out at 600 °C, 2 mL of toluene solution was loaded into the 10 mL cell to give ∼12.4 MPa at the reaction temperature. The sealed reactor was removed from the glovebox and placed into a heating block preheated to 670 °C. The reactor temperature was determined using a thermocouple placed inside the heating block next to the reactor. The reaction cell reached the reaction temperature within 5 min. Fifteen minutes after placing the reactor in the heating block, it was removed from the heating block and cooled rapidly in water bath. The reactor reached room temperature after 5 min in the water bath.

The reaction product consisted of a black solution of nanotubes in toluene. It was collected from the reactor in air. Hexane was used to extract the remaining product that had adhered to the reactor walls. The dispersed product removed from the reactor was centrifuged at 8000 rpm for 10 min to isolate a black precipitate containing the nanotubes. The supernatant was discarded, and the precipitate was redispersed in hexane and centrifuged again. This washing step was repeated once more to ensure that all of the organic molecular byproducts had been separated from the nanotube product.

Characterization. The product was characterized by high-resolution transmission electron microscopy and scanning electron microscopy (HRTEM and HRSEM) and electron energy loss spectroscopy (EELS). For TEM and EELS, the final dry product was redispersed in hexane and dropped onto a lacey carbon-coated TEM grid (Electron Microscopy Sciences). The nanotubes are sufficiently long to span to holey regions of the lacey carbon film, allowing TEM imaging and collection of EELS without a carbon substrate background. This was of primary importance for the EELS measurements, where the background carbon signal obscures the spectroscopic data. A JEOL 2010F operating at 200 kV accelerating voltage was used for TEM imaging and for EELS. The JEOL 2010 F was equipped with a Gatan parallel-EELS spectrometer. Electron energy loss spectra were acquired in STEM mode with the field emission gun operating at 200 keV, with the EELS aperture size set at 2 mm and a camera length of 10 cm, which translates into 5 mrad of collection semiangle. The electron beam size was set at 1 nm for performing the EELS measurements. HRSEM images were obtained on a field emission LEO 1530 SEM operated at 4 kV. For SEM observation, the product was dispersed by brief sonication in hexane and then drop-cast on a piece of silicon wafer (2 cm × 2 cm), which had been washed ultrasonically in ethanol (5 min)−acetone (5 min)−ethanol (5 min) beforehand.

Results

Ferrocene-Catalyzed Nanotube Synthesis. Parts a and b of Figure 1 show HRSEM images of the crude carbonaceous product obtained by degrading toluene at 600 °C and ∼12.4 MPa in the presence of 2.5 mM ferrocene. The product appears as an entangled mesh of fibrous material. TEM images reveal that the wires are a mixture of MWNTs and solid carbon nanofilaments. In the absence of ferrocene, there is no appreciable degradation of toluene at 600 °C at ∼12.4 MPa. HRTEM images of MWNTs and nanofilaments—such as those in Figure 1c−f—show the filament core to consist of randomly stacked graphene sheets (Figure 1e), whereas the nanotubes exhibit coaxially stacked graphene sheets (Figure 1c) with a layer spacing of 0.344 nm, in good agreement with previously reported intertubule spacing.[29] The yield of carbon nanotubes relative to the total carbonaceous material produced in the reaction is approximately 2% based on TEM observations. Catalyst particles were always observed at the tips of the MWNTs and nanofilaments. The fiber morphology—whether the carbon structures end up as tubes or solid filaments—appears

(20) Holmes, J. D.; Johnston, K. P.; Doty, R. C.; Korgel, B. A. *Science* **2000**, *287*, 1471−1473.
(21) Holmes, J. D.; Ziegler, K. J.; Doty, R. C.; Pell, L. E.; Johnston, K. P.; Korgel, B. A. *J. Am. Chem. Soc.* **2001**, *123*, 3743−3748.
(22) Hanrath, T.; Korgel, B. A. *J. Am. Chem. Soc.* **2002**, *124*, 1424−1429.
(23) Hanrath, T.; Korgel, B. A. *Adv. Mater.* **2003**, *15*, 437−440.
(24) Lu, X.; Hanrath, T.; Johnston, K. P.; Korgel, B. A. *Nano Lett.* **2003**, *3*, 93−99.
(25) Davidson, F. M.; Schricker, A. D.; Wiacek, R.; Korgel, B. A. *Adv. Mater.* **2004**, *16*, in press.
(26) Hyeon, T.; Lee, S. S.; Park, J.; Chung, Y.; Na, B. H. *J. Am. Chem. Soc.* **2001**, *123*, 12798−12801.
(27) Sun, S.; Murray, C. B.; Weller, D.; Folks, L.; Moser, A. *Science* **2000**, *287*, 1989−1992.
(28) Yaws, C. L. *Handbook of Thermodynamic Diagrams*; Gulf Publishing Co.: Houston, TX, 1996.
(29) Burian, A.; Dore, J. C.; Fischer, H. E.; Sloan, J. *Phys. Rev. B: Condens. Matter Mater. Phys.* **1999**, *59*, 1665−1668.

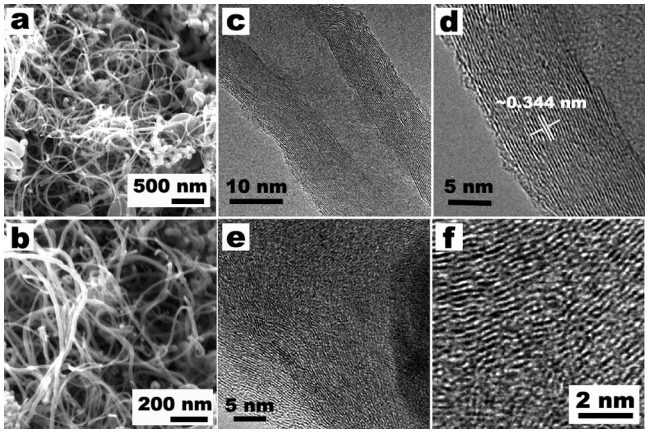

Figure 1. High-resolution scanning electron microscopy (HRSEM) images (a, b) of the crude reaction product consisting of carbon nanofilaments and MWNTs obtained by heating 2.5 mM ferrocene in toluene solutions for 15 min at 600 °C and ~12.4 MPa. HRTEM images of a MWNT (c, d), and a carbon filament (e, f), isolated from the reaction at 600 °C, ~12.4 MPa, using ferrocene as the growth catalyst. The MWNTs exhibit concentrically stacked graphite sheets (d), whereas the nanofilaments exhibit disordered stacking along the length of the filament (f).

to depend on the size and shape of the catalyst particle, with nanotubes being generated from smaller catalytic particles.

After examining the effects of catalyst concentration, hydrocarbon species, reaction pressure, and temperature on the reaction product, the temperature appears to be the most significant parameter in determining the quality of the nanotube product (see the Supporting Information for a complete listing of the experimental results). Figure 2 shows TEM images of product obtained after heating solutions of toluene and ferrocene (2.5 mM) to temperatures ranging from 400 to 650 °C for 15 min, with a reaction pressure of ~12.4 MPa. At 400 °C, the product isolated from the reactor consists only of Fe particles. Toluene does not degrade at this temperature. At 500 °C, larger Fe particles were produced that were coated with a thin layer of amorphous carbonaceous material. The amorphous coating indicates that 500 °C is below the temperature required for graphitization. Fibrous structures, which form at 550 °C, are filamentous but not graphitic. All of these fibers embed Fe particles ranging from 30 to 50 nm in diameter at their tips, indicating that the particles promote fiber formation in the reactor. Interestingly, smaller particles isolated from the reaction mixture did not appear to be associated with the carbonaceous material. Reactions at 600 °C produced MWNTs and graphitic carbon nanofilaments. The optimum reaction temperature for MWNTs was found to be 600 °C. Ferrocene thermally decomposes to form Fe particles, which *catalyze* toluene degradation and promote nanotube and nanofilament formation. Pure toluene is stable at 550 °C and ~12.4 MPa and begins to partially degrade at 600 °C. At 650 °C, toluene degrades rapidly and reactions carried out at 650 °C did not produce filaments or nanotubes. At 650 °C, primarily amorphous carbonaceous material is obtained: the homogeneous solvent pyrolysis rate overwhelms nanotube and nanofilament growth, leading to amorphous particulate formation and catalyst poisoning.

EELS Characterization of Nanotubes and Filaments. Figure 3 shows electron energy loss spectra of an individual multiwall nanotube compared to spectra obtained from a nanofilament. In the experiments, a 1 nm diameter electron beam is scanned radially across the nanotube, while simultaneously

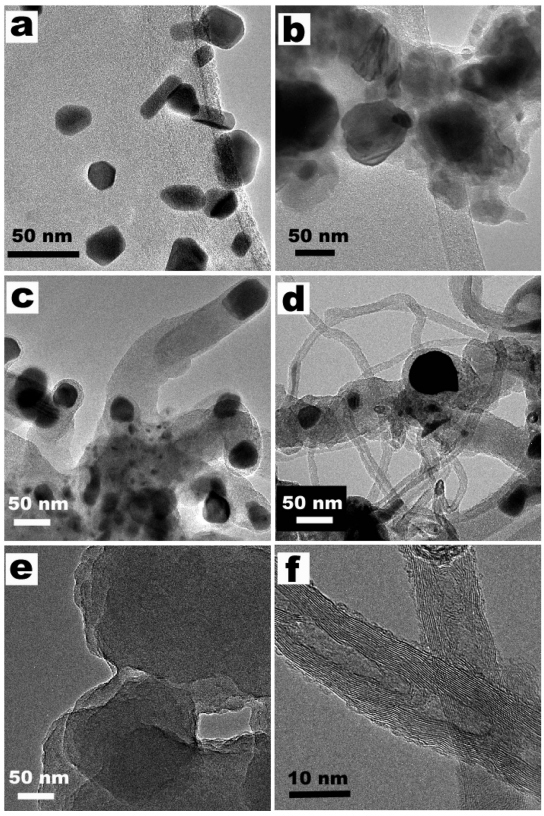

Figure 2. HRTEM images of reaction product obtained at (a) 400, (b) 500, (c) 550, (d) 600, and (e) 650 °C. All reactions were conducted at ~12.4 MPa for 15 min with 2.5 mM ferrocene in toluene loaded into the cell. At temperatures lower than 500 °C, only Fe particles were produced. At 550 °C, amorphous carbon fibers with Fe particles embedded at their tips were produced. At 600 °C, multiwall carbon nanotubes were produced. At 650 °C, severe toluene degradation results in the production of mostly carbonaceous byproduct without MWNTs. Panel f shows enlarged images of the nanotubes in d.

collecting EELS data as a function of probe position. These EELS line scans confirm that the structure in Figure 3a is a multiwall nanotube and the structure in Figure 3b is a nanofilament. EELS spectra taken in the low-loss region exhibit two plasmon peaks corresponding to inelastic electron scattering from collective oscillations (plasmons) of π (~6 eV) and $\pi + \sigma$ (~26 eV) valence electrons. The key differences in the nanotube and filament spectra appear when the electron beam is positioned at the outer edge of the structures. For the MWNT, the $\pi + \sigma$ plasmon shifts to significantly lower energy—approximately 18 eV—when the probe is positioned at the nanotube surface. An additional lower lying sideband at approximately 14 eV also appears in the spectra. In the nanofilament, the $\pi + \sigma$ plasmon energy does not depend on the probe position. Energy-dispersive X-ray spectroscopy (EDS) did not reveal the presence of any impurities, such as iron debris from catalyst, and furthermore the peak shift is not due to a change in carbon−carbon bonding. The peak shifting that occurs in the nanotube EELS spectra is the result of the anisotropic symmetry of the π electrons delocalized parallel to the graphene sheets in the nanotube wall. Due to the plasmon dispersion relation, when the beam is positioned orthogonally incident to a (002) graphite plane, as is the case in the center of the nanotube, the $\pi + \sigma$ plasmon energy is 26.5 eV. When the beam is positioned at the nanotube edge, the beam is directed parallel to the graphitic sheets, resulting in a lower energy plasmon peak

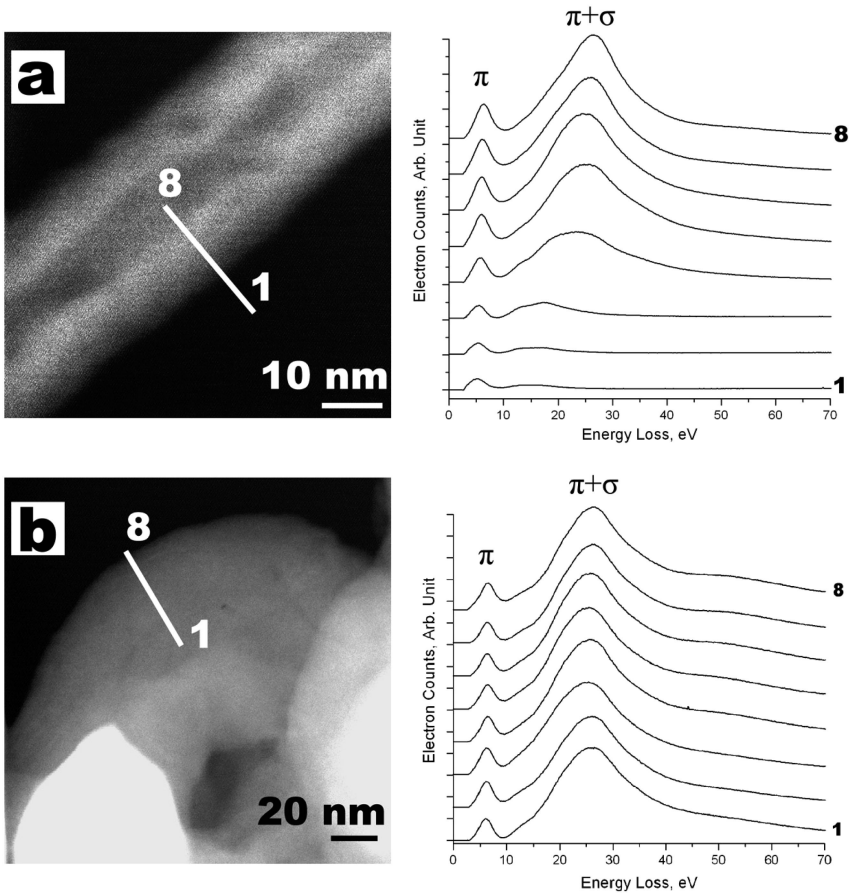

Figure 3. Dark-field TEM images and EELS line scans across (a) a multiwall nanotube and (b) a carbon nanofilament. The numbered labels on the spectra correspond to the labeled axial positions in the corresponding TEM image.

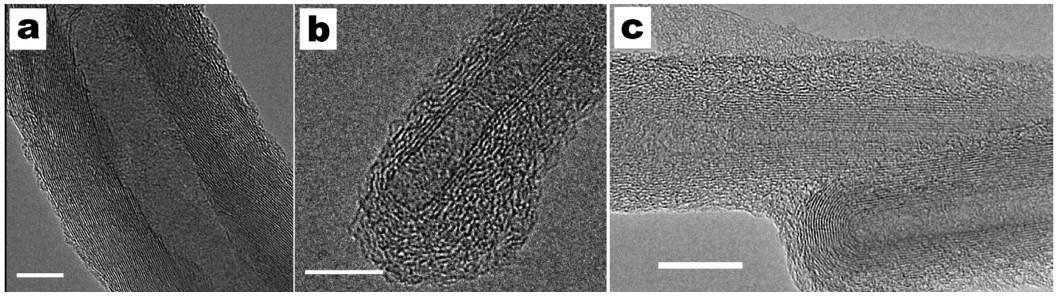

Figure 4. MWNTs formed from toluene catalyzed using (a) ferrocene, (b) Fe nanocrystals (9.2 nm diameter), and (c) FePt nanocrystals (4 nm diameter). All reactions are carried out at 600 °C, ~12.4 MPa, for 15 min. Scale bars are 10 nm.

position. Results from angle-dependent EELS measurements from graphite are well-known, and our measurements match the expected values for the plasmon energies at both the center (orthogonal to the (002) plane) and surface (parallel to the (002) plane) of the nanotubes.[30] The plasmon energy does not shift as a function of probe position in the nanofilament since the graphitic carbon is randomly oriented. The EELS spectra clearly demonstrate that MWNTs were obtained from these reactions.

Fe and FePt Nanocrystal-Seeded MWNT Formation. MWNTs were also synthesized by direct injection of sterically stabilized Fe and FePt nanocrystals. The Fe and FePt particles were injected with diameters less than 10 nm, which is significantly less than the 20−50 nm diameter Fe particles formed by in situ ferrocene degradation. The MWNTs generated using the preformed catalyst particles were generally of smaller diameter, reflecting the more stable smaller diameter seed particles; however, the nanotube yield was lower. Figure 4 shows high-resolution TEM bright-field images of carbon nanotubes grown using the different catalysts. The smaller MWNTs were typically straighter than the larger tubes, most likely as a result of greater surface stress due to the increased curvature of the graphite sheets in the nanotube shell.[31,32] The lower yield could be due to the adsorbed organic passivation layer on the nanocrystals, which initially could potentially inhibit surface-directed nanotube growth, or smaller diameter nanotube formation may simply be less efficient under these low temperature growth conditions. Although smaller nanotubes

(30) Zeppenfeld, K. *Z. Phys.* **1968**, *211*, 391−399.

(31) Kim, N. S.; Lee, Y. T.; Park, J.; Han, J. B.; Choi, Y. S.; Choi, S. Y.; Choo, J. B.; Lee, G. H. *J. Phys. Chem. B* **2003**, *107*, 9249−9255.

(32) Dai, H.; Rinzler, A. G.; Nikolaev, P.; Thess, A.; Colbert, D. T.; Smalley, R. E. *Chem. Phys. Lett.* **1996**, *260*, 471−475.

should form more efficiently at higher reaction temperatures, we could not explore this possibility since the homogeneous solvent degradation at 650 °C and above eliminated nanotube formation, thus preventing the exploration of a wider range of synthetic temperatures in this system.

Discussion

Role of Catalyst in MWNT Formation. Fe catalyst particles were observed at the ends of the nanotubes and the filaments grown using ferrocene injection. Transition metal particle catalyzed carbon filament and nanotube growth has been extensively studied since the 1950s, and a few critical steps in the carbon filament formation process are well-known:[33,34] (1) catalytic hydrocarbon decomposition occurs at the particle surface, which results in (2) carbidization of the catalyst, subsequently saturating the particle with carbon and giving rise to (3) surface-directed graphitization and nanotube or nanofilament formation. Figure 5 shows a schematic representation of the growth process. Although the mechanistic steps have been identified, many important details about nanotube formation are still not well understood. For example, carbon will alloy with the Fe particle but may be associated with either the Fe nanoparticle surface or the interior of the particle. And nanotube growth itself has been proposed to occur by either "root growth",[32] in which the nanotube base interfaces directly with the nanoparticle, or a "folded growth mode",[35] in which the carbon shell that forms the nanotube wraps around the nanoparticle leading to the curved graphitic layers that extrude from the particle surface. In fact, it appears from extensive data in the literature that both of these mechanisms can occur depending on the synthetic conditions.[32,35] Information about the growth mechanism in the supercritical solvent can be deduced by examining the particle tips of the nanotubes and filaments.

Figure 6 shows two representative TEM images of the catalyst particles at the end of a MWNT and a carbon filament, along with the fast Fourier transform (FFT) of the image. We observed two primary differences between particles associated with nanotubes and those associated with filaments. First, the particles associated with the nanotubes were smaller: nanotubes had particles less than 30 nm in diameter, whereas larger particles were attached to filaments. Second, the seed particle compositions of nanotubes and filaments were different: the particles at the tips of the nanotubes were composed of pure fcc Fe, while the particles at the end of the nanofilaments were composed of an Fe−C alloy. Both seed particles are coated with a carbon shell. However, the filament seed particles exhibit a thin Fe−C shell that surrounds the particle core, which appears to be composed of a different Fe−C composition or structure. The Fe seed particle embedded at the tip of the MWNT interfaces directly with the graphitic carbon shell.

On the basis of TEM observations, it appears that the nanotubes produced in supercritical toluene form by the folded-growth mechanism, whereas the nanofilaments grow by a VLS-type (vapor−liquid−solid) mechanism. In our laboratory, we have exploited the VLS mechanism to produce Si,[20,24] Ge,[22,23] and GaAs[25] nanowires in supercritical solvents using gold nanocrystals to seed growth, a process termed supercritical fluid−liquid−solid (SFLS) growth. The carbon filaments produced in supercritical toluene form by this mechanism, with the exception that the seed particles may be a solid Fe−C alloy, instead of a liquid, since the growth temperatures are well below the Fe−C eutectic temperature. However, nanometer-size particles exhibit a melting point depression, which means that a liquid-phase seed particle cannot be entirely ruled out. Regardless, the only requirement from VLS-type growth from nanometer particles is limited solubility of the wire material in the seed. The fact that the graphitic layers in the carbon nanofilament cores form disordered stacks oriented orthogonal to the growth direction further supports the idea that the filaments form at the surface of a metal seed.

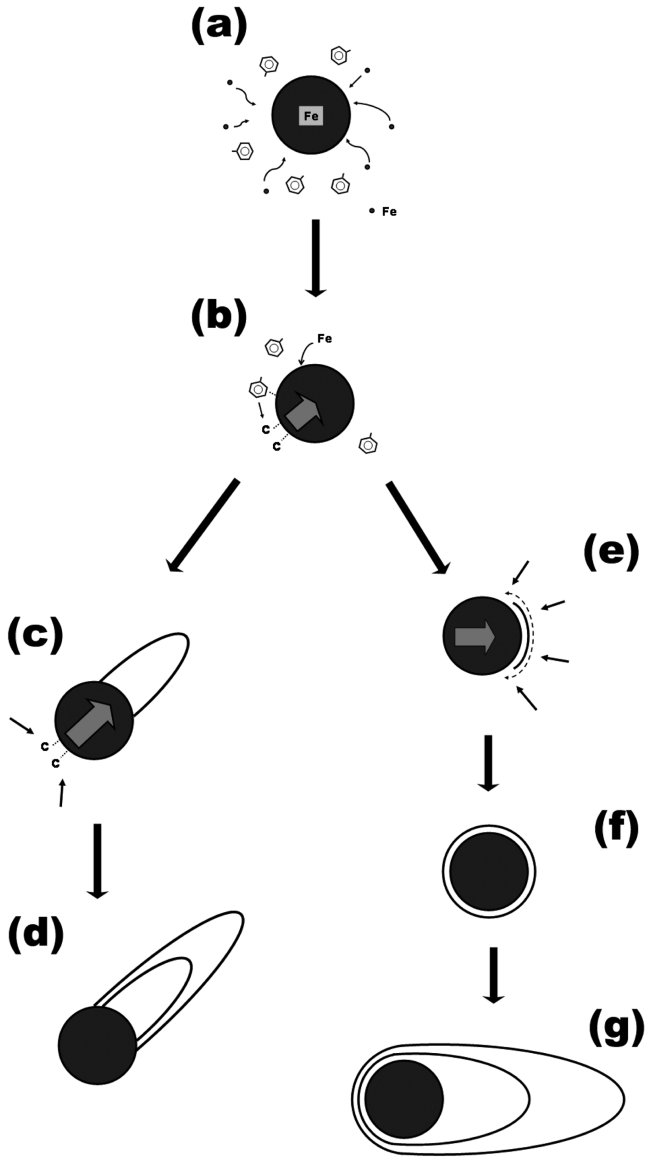

Figure 5. Schematic representation of the nanotube growth process. (a) Hydrocarbon decomposes at the catalytic surface. (b) Decomposed carbon diffuses into the nanoparticle and eventually saturates the catalyst. Surface-directed graphitization can take place mainly in two ways: (c−d) "root growth mechanism",[32] where the nanotube edge is bound to the surface of the catalyst and the nanotube wall is thrust up with a continuous supply of carbon source; (e−g) "folded growth mode",[35] where graphitic nanosheets evolve as carbon precipitates on the catalyst surface. Nanotubes grown in the present study exhibit particles embedded at the tip, indicating that the folded growth mode dominates in our case.

(33) Evans, E. L.; Thomas, J. M.; Thrower, P. A.; Walker, P. L. *Carbon* **1973**, *11*, 441−445.
(34) Bower, C.; Zhou, O.; Zhu, W.; Werder, D. J.; Jin, S. *Appl. Phys. Lett.* **2000**, *77*, 2767−2769.
(35) Louchev, O. A.; Hester, J. R. *J. Appl. Phys.* **2003**, *94*, 2002−2010.

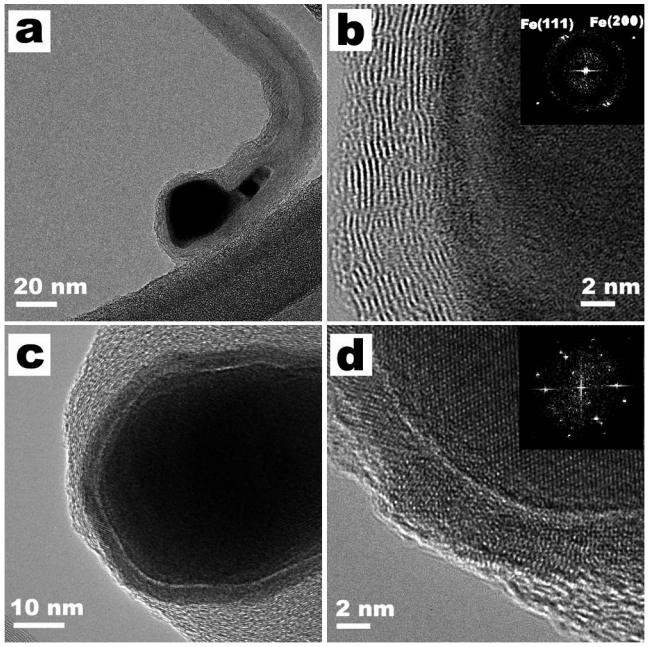

Figure 6. HRTEM images of catalyst particles at the tip of a MWNT (a, b), and a carbon filament (c, d), produced at 600 °C, ~12.4 MPa, using ferrocene as the catalyst. The particle at the nanotube tip is Fe, while the particle in the nanofilament has a core−shell structure with a crystal structure different from pure Fe. Insets in b and d show FFTs of the HRTEM images. FFTs of the Fe−C alloy seeds, as in d, do not match any Fe or Fe−C alloy crystal structure available from the literature; however, the presence of both Fe and C are confirmed by EDS.

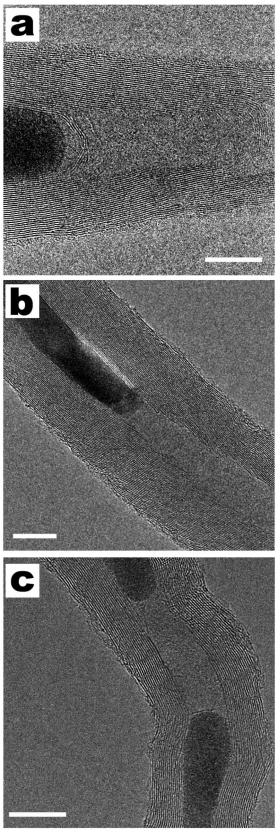

Figure 7. HRTEM images of (a) an embryonic MWNT, (b) a fully grown MWNT, and (c) a MWNT with two Fe particles trapped inside the nanotube. Scale bars are 10 nm.

In order for *nanotubes* to form, the graphitic layers must be curved by the seed particle. The higher surface curvature of the smaller seed particles presumably adds the needed driving force to induce nanotube formation. Below some critical particle diameter, the relatively strong van der Waals attraction between the condensing graphite sheets and the nanoparticle surface stabilizes the formation of hollow nanotubes.[35] Surface-templated graphite sheet formation is clearly evident in the TEM image of the Fe particle at the MWNT tip in Figure 6. Figure 7 shows additional TEM images of MWNTs that reveal the tube morphology near the seed particle. In the folded-growth mechanism, a graphene cap forms at the particle surface, and the carbon layers extend as additional carbon diffuses through the graphitic shell to reach the Fe−nanotube interface. We did not find evidence of the root-growth mechanism for nanotube formation.

The carbon content in the seed particles of different size most likely plays a significant role in determining the nanotube and nanofilament morphology as well. The larger seed particles exhibit higher carbon content, which could favor filament formation due to enhanced wetting between the graphite layers and the seed particle that makes nanotube formation less energetically favorable over filament formation.[36]

Although we certainly tried, we did not produce SWNT under any of the conditions we explored. This does not appear to be a problem related to the seed particle diameter in the reactor but rather a limitation imposed by the relatively low temperatures available in supercritical toluene. Homogeneous solvent degradation at temperatures much higher than ~625 °C completely quenches nanotube and nanofilament formation. In the available temperature window <~625 °C, the thermal energy cannot overcome the higher energetic barrier (relative to MWNTs) to surface curvature needed to produce SWNTs. This curvature energy relates to the critical radius of the nanotube nucleus that forms on the particle surface. At low temperatures, the critical radius of the nucleus is simply too large to permit SWNT formation. In metal-particle-catalyzed CVD, higher reaction temperatures are reached by using methane and CO as precursors, which are relatively stable to homogeneous decomposition, yet degrade catalytically at the particle surface.[12,13,37,38] Other potential supercritical solvents available for nanotube formation that could help limit homogeneous precursor degradation are water and CO_2. These two solvents provide different engineering and safety challenges that must be addressed; however, there is no fundamental reason to believe that the supercritical approach to nanotube formation could not be successful for SWNTs as well as MWNTs.

Summary

Carbon MWNTs and nanofilaments can be produced in supercritical toluene using either the molecular additive, ferrocene, or prefabricated sterically stabilized nanocrystals of Fe or FePt, to catalyze their growth. The carbon nanostructure morphology depends on the reaction temperature and the seed particle size. The temperature must be sufficiently high for (1) significant hydrocarbon decomposition, which occurs *hetero-*

(36) Kuznetsov, V. L.; Usoltseva, A. N.; Chuvilin, A. L.; Obraztsova, E. D.; Bonard, J. M. *Phys. Rev. B: Condens. Matter Mater. Phys.* **2001**, *64*, 235401.
(37) Kong, J.; Cassell, A. M.; Dai, H. *Chem. Phys. Lett.* **1998**, *292*, 567−574.
(38) Kong, J.; Soh, H. T.; Cassell, A. M.; Quate, C. F.; Dai, H. *Nature* **1998**, *395*, 878−881.

geneously at the particle surfaces at temperatures exceeding at least 500 °C for toluene, and (2) carbon graphitization at the metal seed particle surface, which requires temperatures greater than ∼550 °C. At temperatures much exceeding ∼625 °C, homogeneous solvent decomposition spoils nanotube growth. Smaller seed particles (<∼30 nm diameter) promote MWNT formation, while larger particles produce nanofilaments with disorderd graphitic cores.

The supercritical fluid approach to carbon nanotube synthesis has the potential for much higher throughput relative to the heterogeneous gas-phase approaches. However, the quality of the nanotubes currently does not match that of nanotubes produced in the vapor phase. There are many scientific and engineering considerations in process optimization, including reactor design, as well as optimization of catalyst and precursor reactivity. In comparison to the vapor-phase process, which has been studied and optimized by many researchers over the past 10 years, little effort has been spent developing wet nanotube synthesis. One currently open question in the supercritical fluid approach relates to single-wall nanotube growth. Considering that SWNTs are known to require more energy to form than MWNTs, the use of thermally stable alternative supercritical solvents, e.g. supercritical CO_2, could improve the quality of nanotubes, eventually leading to SWNT formation. The use of these kinds of supercritical solvents could also improve MWNT yield by limiting homogeneous solvent decomposition and catalyst poisoning at higher temperature.

Acknowledgment. We thank the National Science Foundation (NSF), the Welch Foundation, and the Texas Higher Education Coordinating Board (ATP program) for financial support of this work. We are grateful to M. Jose-Yacaman, T. Hanrath, and A. E. Saunders for fruitful discussions, and we thank J. P. Zhou for assistance with the EELS and TEM measurements.

Supporting Information Available: Description of the reaction products from different reaction conditions (Table S1). This material is available free of charge via the Internet at http://pubs.acs.org.

JA031522S